Available online at www.eccomasproceedia.org
Eccomas Proceedia COMPDYN (2025) 67-78

ECCOMAS
Proceedia

COMPDYN 2025
10th ECCOMAS Thematic Conference on
Computational Methods in Structural Dynamics and Earthquake Engineering
M. Papadrakakis, M. Fragiadakis (eds.)
Rhodes Island, Greece, 15-18 June 2025

EXPERIMENTAL AND NUMERICAL ANALYSIS OF A SUBSTRUCTURE SYSTEM OF A FULLY PRECAST BRIDGE UNDER HORIZONTAL CYCLIC LOADS

L. Carvalho[1], M. Pimentel[1], A. Arêde[1] and P. Delgado[2,1]

[1] CONSTRUCT, Faculty of Engineering, University of Porto
R. Dr. Roberto Frias, s/n 4200-465, Porto, Portugal
e-mail: lucasc@fe.up.pt, mjsp@fe.up.pt, aarede@fe.up.pt

[2] proMetheus, Instituto Politécnico de Viana do Castelo
R. Escola Industrial e Comercial de Nun´Álvares, 4900-347, Viana do Castelo, Portugal
e-mail: pdelgado@estg.ipvc.pt

Abstract

Prefabricated systems enable the industrialization of bridges, enhancing efficiency in construction processes, being a topic of increasing interest. However, current European design standards are based on cast-in-place structures, and their construction provisions are not always suitable to prefabricated ones. In areas of greater seismicity, current standards often lead to reinforcement congestion, mainly in the joint zones (column-to-cap beam and columns-to-foundation), making the assembly process of prefabricated elements difficult and unworkable, limiting their use and restraining the benefits the industrialization provides. Given this, some strut-and-tie models were developed to enable alternative and simplified reinforcement layouts within the joint zone, providing a suitable solution for prefabrication in seismic zones. These models were applied in the design of a case study, a double-track railway viaduct with six spans (22m + 4x30m + 22m) and columns with 10m high, from the top of the foundation to the base of the cap beam. Experimental analysis of four reduced-scale test specimens (1:3,6) of the developed solution under horizontal cyclic loading has been carried out, aiming to confirm the adequacy of the design and the proposed solution. This paper focuses on a nonlinear numerical analysis to reproduce the experimental behavior, aiming to assess the redistribution of forces in the joints, allowing the extrapolation of the experimental results to alternative geometries and reinforcement layouts. As a modeling strategy, a rotating smeared crack model was considered. Theoretical constitutive curves with fracture energy were adopted to simulate the concrete mechanical behavior. The Menegotto-Pinto model was applied to simulate the reinforcement behavior under cyclic load conditions.

Keywords: Bridges, Beam-column joints, Numerical models, Seismic behavior, Pre-cast solutions.

ISSN:2623-3347
Peer-review under responsibility of the organizing committee of COMPDYN 2025.
doi: 10.7712/120125.12392.26008

1 INTRODUCTION

Industrialization offers the opportunity to enhance the construction process of bridges and viaducts through prefabricated structures. This approach allows to meet tight deadlines, reduce traffic interruptions, and enhance worker safety. In the context of industrialization in seismic zones, prefabricated structures have been well accepted in low seismicity areas but have faced reluctance to be applied in moderate to high ones. This lies in uncertainties related to their performance to withstand earthquakes of such intensity. Part of this can be attributed to the fact that European standards have been developed focusing on in-situ structures solutions, which are not immediately applicable to precast ones, leading the established construction provisions difficult to fit into the prefabricated context.

The awareness concerning this subject has led to a growth in research related to the assessment of precast structures to withstand earthquakes of greater intensity. Connection systems between precast elements have been developed and evaluated [1-9], aiming to ensure a monolithic behavior like the cast-in-place ones, allowing to adhere to current standards in the design process of precast structures. Research on the force transfer mechanism between column-beam and column-foundation connections has been conducted [10-13], to promote more efficient construction arrangements, avoid reinforcement overlapping issues, and ensure a reliable path of force transfer between structural elements.

In this paper, section 2 briefly presents a fully precast substructure solution developed to withstand a seismic acceleration of 2,25 m/s^2, along with their simplicity in assembly and execution on site [10]. Section 3 presents the geometry and reinforcement layout of the test specimen PE0, on a reduced scale of 1:3,6, of the substructure solution presented. Section 4 introduces the numerical model developed and the constitutive models used to faithfully reproduce the structural behavior observed in the experimental test. This makes it possible to extrapolate the experimental results to alternative geometries and reinforcement layouts, while avoiding time loss and high costs that experimental tests require. Section 5 is devoted to analyzing the numerical results achieved with their corresponding experimental data.

2 SUBSTRUCTURE SOLUTION FOR PERFORMANCE AND CONSTRUCTABILITY

The case study providing the context for the substructure solution developed is a double-track railway viaduct with 6 spans of 22 m + 4 x 30 m + 22 m, Figure 1. The continuous deck is bearing supported on 5 intermediate cap-beams with two columns each. As shown in Figure 2, the columns are 10m high between the top of the foundation and the base of the cap beam. The deck is constituted by 4 precast longitudinal U-beams in each span. It was considered that the support devices on the cap-beam do not transmit longitudinal forces. Thus, the substructure system is responsible for the seismic action resistance in the transverse direction, being the transverse forces from the deck transferred through a corbel at the center of the cap-beam. The longitudinal seismic forces are balanced at the abutments by dedicated dissipative devices.

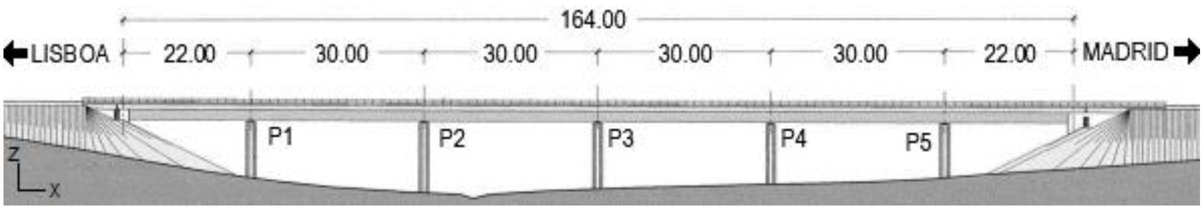

Figure 1: Analyzed Viaduct.

(a) transversal view. (b) perspective of the bridge.

Figure 2: Two-column bents layout.

A force-based design approach was adopted in the design, i.e., the columns were designed for maximum forces developed through a response spectrum analysis in SAP2000 [14], considering an acceleration of 2,25 m/s^2. These seismic forces were determined considering an inelastic design spectrum with a behavior factor q = 3,0. Overall, the structure was designed to meet the basic requirements of non-collapse and minimization of damage, as required in the European standards [15-16]. To fulfill these requirements, the capacity design approach was used to ensure a ductile structural behavior, allowing the formation of plastic hinges on the column ends and avoiding brittle failure by proper confinement.

The cap-beam geometry was defined considering weight constraints, and the dimensions needed to accommodate the final and temporary bearings during the assembly process. As a fully precast solution is envisaged, a cap-beam-to-column connection system was conceived utilizing corrugated ducts distributed accordingly with the layout of the column vertical bars, allowing a streamlined on-site assembly process. These ducts are posteriorly grouted for the anchorage of the vertical bars. Special attention was paid to the reinforcement layout at the cap-beam-to-columns joints. These are discontinuity regions, and the design was performed resorting to strut-and-tie models [17], allowing a reasonable reinforcement ratio to avoid too dense reinforcement in these zones.

The columns were designed to accommodate the transversal seismic forces with a longitudinal reinforcement ratio of about 1.2 %, which ensures the viability of using corrugated ducts with diameters of 80 mm to 100 mm. The minimum transversal stiffness of the railway bridge complying with the Eurocode 1 [18] requirements for high-speed railway lines was also verified. In the longitudinal direction, the columns work as cantilevers and the corresponding second order effects govern the minimum dimension of the columns.

3 REDUCED SCALE TEST SPECIMEN

Experimental tests to assess the conceived substructure system started with the PE0 prototype. The Cauchy similitude relationship was used to scale the structure to 1:3,6 relative to the full-scale version, as shown in Figures 3, 4, and 5. It is noteworthy that PE0 columns are hinged at mid-height, at the section of null flexural moment. The experimental test was based on cyclic horizontal loading until failure, with the horizontal forces applied to the corbel located at the top of the cap-beam, and vertical forces considered constants and distributed at four points on the cap-beam, aiming to represent the mobilized mass under a cyclic event.

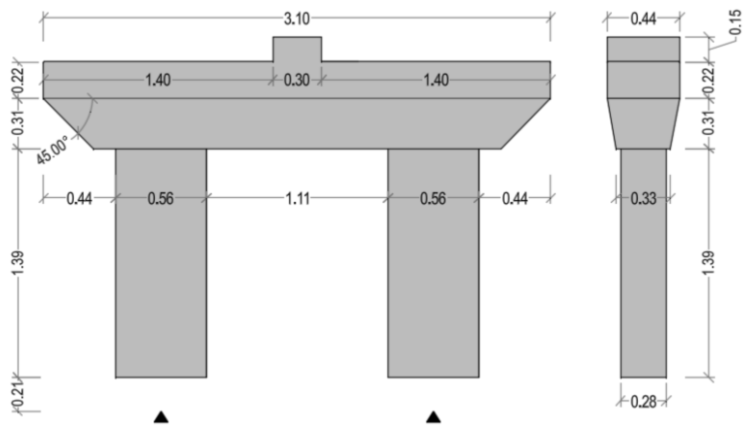

Figure 3: PE0 geometry.

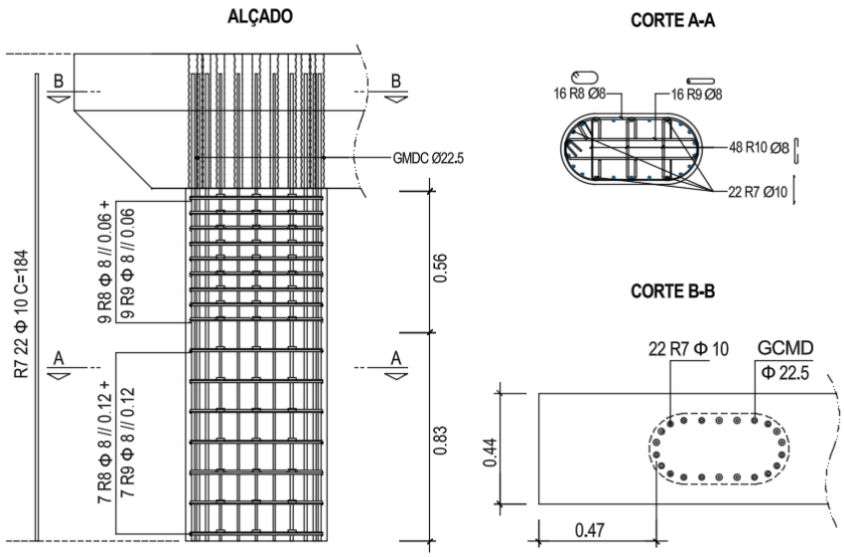

Figure 4: Column reinforcement layout.

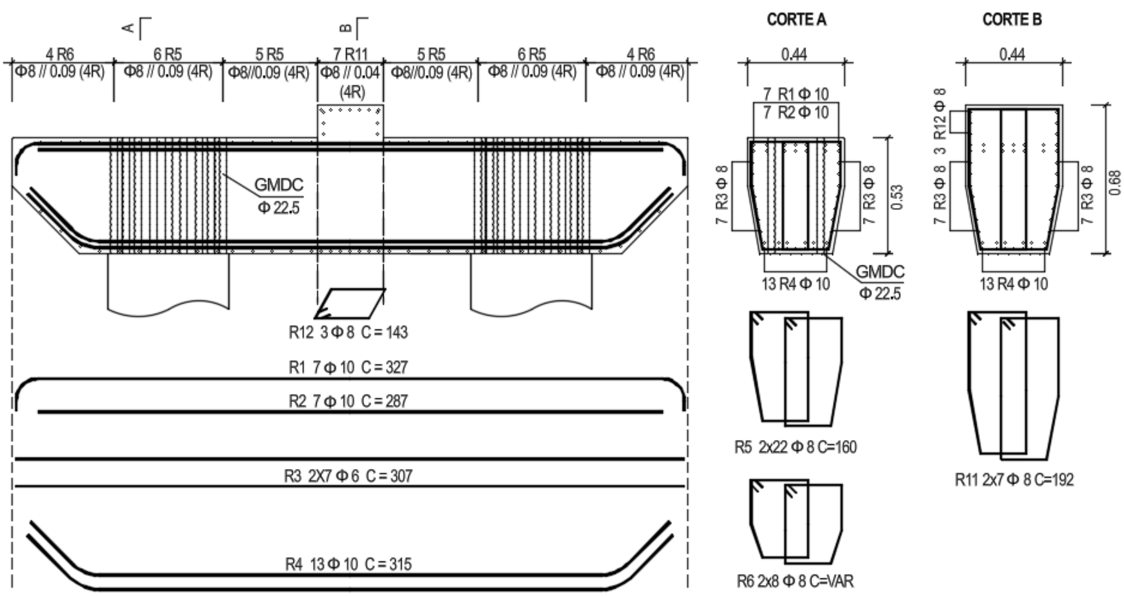

Figure 5: Cap-beam reinforcement layout.

The values of the most relevant properties of the materials used in the construction of the test prototype PE0 are those listed in Table 1. SikaGrout-340 and SikaDur-30 were used to assemble the connections between columns and cap-beam: SikaGrout-340 was used to fill the metallic ducts, while Sikadur-30, a bi-component mixture, was applied to the column-to-cap-beam interface.

Material	$f_{c,cube}$ (MPa)	f_y (MPa)	f_u (MPa)	ε_u (%)	E_s (MPa)
Concrete	70	-	-	-	-
SikaGrout-340	95	-	-	-	-
SikaGrout-30	90	-	-	-	-
Reinforcement ϕ8	-	666	725	4,75	177860
Reinforcement ϕ10	-	539	639	13,40	180874

Table 1: Material properties.

4 NONLINEAR NUMERICAL ANALYSIS

A three-dimensional finite element model, that can be seen in Figure 6, was developed in the software DIANA 10.5 [19] to assess the performance and emulate the behavior of the reduced scale prototypes. It is important to note that ZX is a symmetry plane, where only half of the structure is modeled, thus supports were provided to simulate this effect. The mesh consists in linear hexahedral elements of eight nodes, with size of approximately 25 mm. The material properties are that corresponding to Table 1 (noting that, since cubic specimens were used to estimate the compressive strength of the concrete, a value of 0,7 x $f_{c,cube}$ was adopted). All the reinforcements were explicitly included in the model, where transversal reinforcements are considered embedded, sharing the same displacement field of the concrete embedding elements, while the longitudinal bars include bond-slip elements. Interface elements with no tension and shear stiffness reduction were considered to simulate the column-to-cap-beam connection zone behavior.

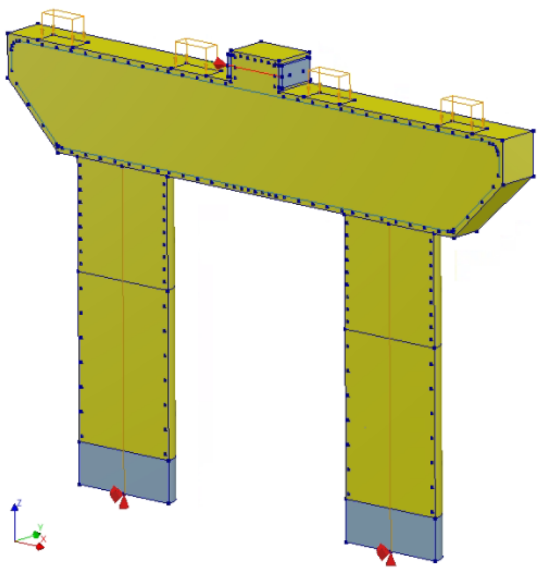

(a) geometry and loads configuration.

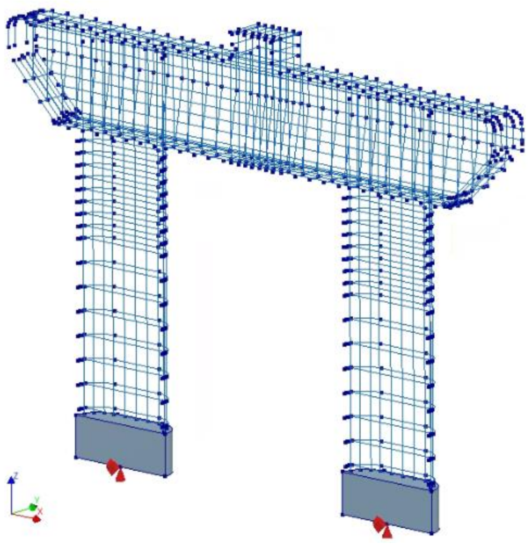

(b) reinforcements.

Figure 6: Numerical model.

4.1 Constitutive models for concrete

To simulate the cracked concrete, a total strain based rotating smeared crack model was used, which has shown a good performance in horizontal cyclic simulations where the structure exhibits a distributed cracking pattern. The rotating crack model [20] considered has as its main assumption the reorientation of two axes of orthotropy according to the change in the crack orientation, always coinciding with the main deformation directions, leading to the advantage of having always shear stresses equal to zero, and thus avoiding the necessity of a law to describe the relationship between shear stresses and distortions.

To consider the nonlinear compression response in the modeling, a parabolic uniaxial compressive stress-strain curve [21] showed in Figure 7 was selected, including a regularized post-peak branch defined by the compressive fracture energy, G_C = 90 N/mm. The Hsieh-Ting-Chen failure envelope and multiaxial compressive stress states were adopted, as described in [22], allowing to restrict the transverse deformation of an element subject to axial compression, increasing the compression strength and the deformation capacity of the element, thus translating into a greater ductility capacity.

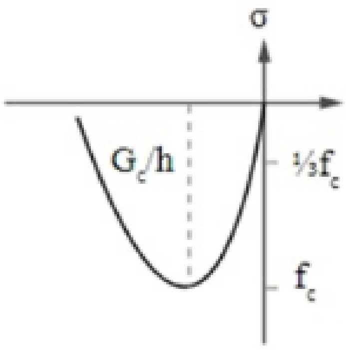

Figure 7: Parabolic curve [21].

The crack band model was used to model tensile fracture. The strain softening curve is that proposed by Hordijk [23], showed in Figure 8, defined by the tensile strength, f_t = 3,0 MPa and by the fracture energy, G_F = 0,15 N/mm. The curve adopted aims to reproduce the decrease in tensile stresses in concrete as the width of the crack increases, since concrete is able to transmit residual stresses while the cracks are not fully formed. Also, the reduction of the Poisson effect due to cracking was considered in the model. When a crack is completely formed the Poisson effect is null, and therefore disregarding the reduction of the Poisson effect in which there is an important cracking process can cause a large error in estimating the structure deformations.

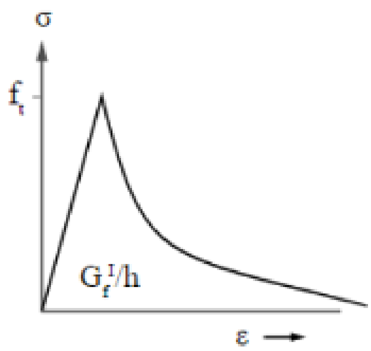

Figure 8: Hordijk curve [23].

4.2 Constitutive model for reinforcement

The stress-strain relationship used to simulate the non-linearity of the reinforcements under horizontal cyclic loading is the Menegotto-Pinto model [24], showed in Figure 9. The parameters values used to define the curve are those presented in Table 2.

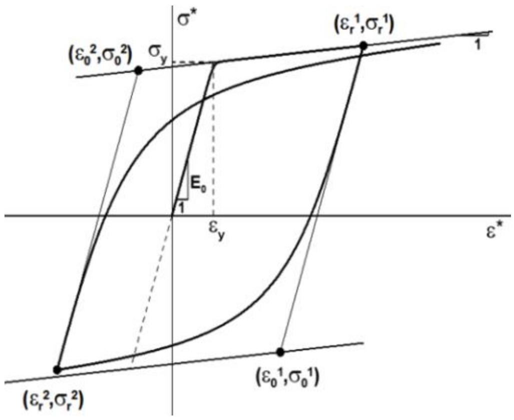

Figure 9: Menegotto-Pinto model [24].

Initial tangent slop ratio – E_0	0.03
Initial curvature parameter - R_0	20
Constant a_1	18.5
Constant a_2	0.15
Constant a_3	0.01
Constant a_4	7

Table 2: Parameters.

The parameters listed in Table 2 are dimensionless. It is worth mentioning that, in DIANA FEA, the initial tangent slope ratio (E_0) is normalized in relation to the yield stress of the reinforcement (f_y), resulting in the relationship presented in equation 1:

$$\frac{1}{E_0} = \frac{\varepsilon_y}{f_y} \quad \Rightarrow \quad \varepsilon_y = \frac{f_y}{E_0} \tag{1}$$

The other parameters, such as the initial curvature (R_0), which influences the transition smoothness between the elastic and plastic behavior, and the constants a_1, a_2, a_3 and a_4, can be adjusted empirically. However, the values adopted were based on previous analysis [25].

4.3 Constitutive model for bond-stress transfer

The bond stress-slip relationship was incorporated into the numerical model through the curve proposed by the fib Model Code 2010 [26], showed in Figure 10. It was considered the maximum bond shear stress (τ_{bmax}) equal to 9,5 MN/m^2 for a slip (S_1) of 1,0 mm.

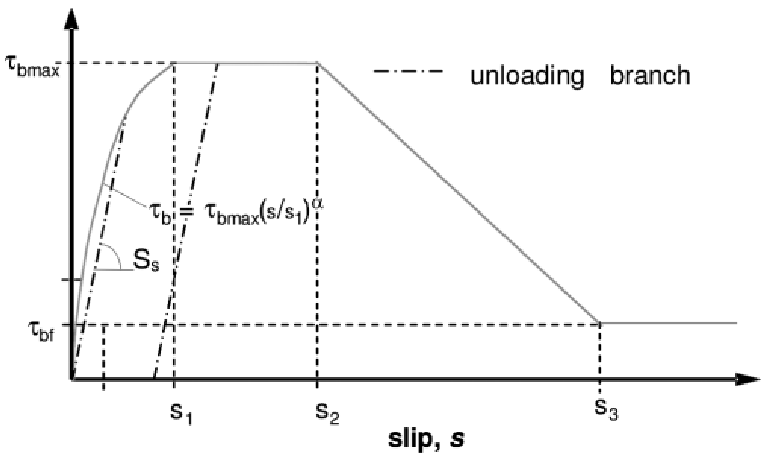

Figure 10: Bond stress-slip relationship [26].

5 NUMERICAL AND EXPERIMENTAL RESULTS

5.1 Hysteretic Response

Figure 11 (a) shows the lateral force vs. displacement hysteretic curve from the experimental test and the corresponding result achieved in the numerical analysis. In addition, Figure 11 (b) shows the backbone curve for both analyses. The drift was calculated considering the distance between the axis of the hinged base and the column-to-cap-beam interface.

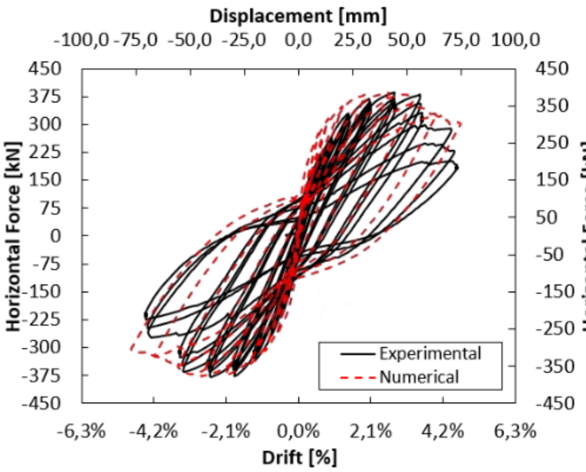

(a) hysteretic curve.

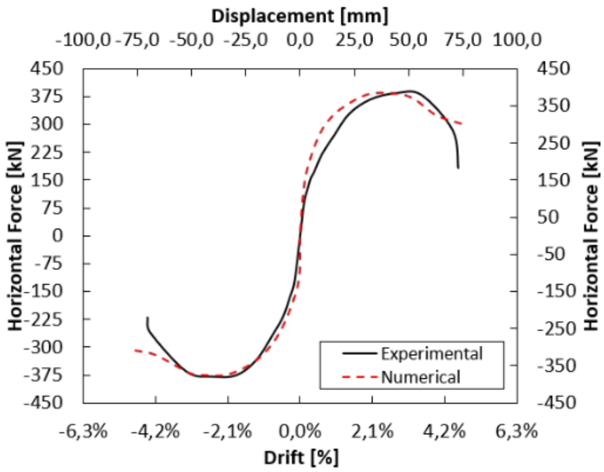

(b) backbone curve.

Figure 11: Horizontal force vs. lateral displacement– comparison between numerical and experimental data.

Based on the results presented in Figure 11, the fully precast solution conceived had a satisfactory performance during the experimental test, with gradual damage evolution and ductile behavior. It is possible to observe the formation of the plastic mechanism through the yielding plateau, as well as the capacity to withstand several hysteresis cycles maintaining a residual strength capacity. The structural failure was ductile and occurred for a high drift level. The nonlinear numerical analysis effectively simulated the structural behavior observed in the experimental test, showing good agreement. The analysis gathered key phenomena such as stiffness degradation between cycles, energy dissipation, and the maximum horizontal force achieved. However, some small divergences between the numerical and experimental results can be noted, such as the initial stiffness and the transition point between the elastic and plastic regimes. Regarding the initial stiffness, it was expected to obtain a higher value in the numerical analysis, since the experimental test includes inevitable accommodations and deformations of the steel elements that transfer the horizontal forces from the actuator to the specimen, and the monitoring system is unable to ignore these effects. Concerning the transition point between the elastic and plastic regimes, this phenomenon is evident for the horizontal demand, whereas for the negative horizontal demand, the transition point coincides with good accuracy. Similar to the initial stiffness issue, the accommodations and deformations in the experimental setup probably contribute to these divergences.

5.2 Damage Evolution and Failure Mode

Figures 12 to 15 present the evolution of the structural damage throughout the experimental test and the corresponding result achieved in the numerical analysis. This includes key drift levels where important cracking progression, concrete crushing and reinforcement exposure can be noted, enabling a comprehensive comparison with the corresponding numerical results and their accuracy in replicate the reality. Noting that the numerical results are only presenting the response to the rightward horizontal demand. However, this is a seismic analysis in which both column sides experienced similar degradation.

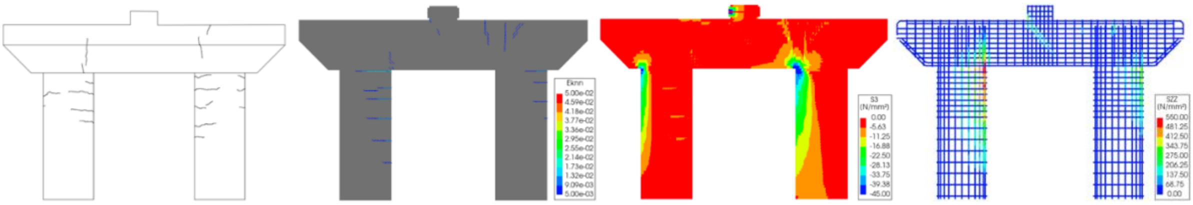

(a) experimental - cracking pattern. (b) numerical - cracking pattern. (c) numerical – principal compressive stress field. (d) numerical – vertical bar stresses.

Figure 12: Damage at 0.69 % drift – 11 mm of displacement.

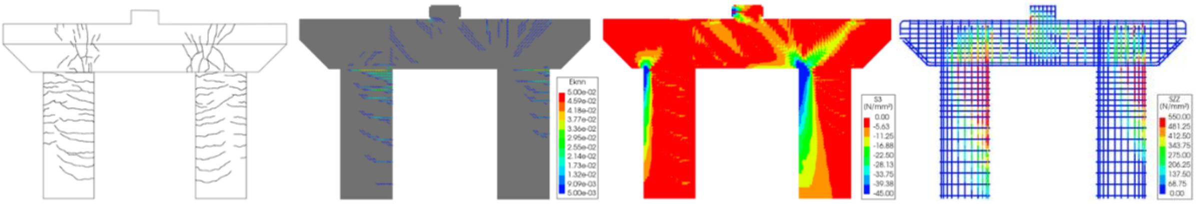

(a) experimental - cracking pattern. (b) numerical - cracking pattern. (c) numerical – principal compressive stress field. (d) numerical – vertical bar stresses.

Figure 13: Damage at 2.08 % drift – 33 mm of displacement.

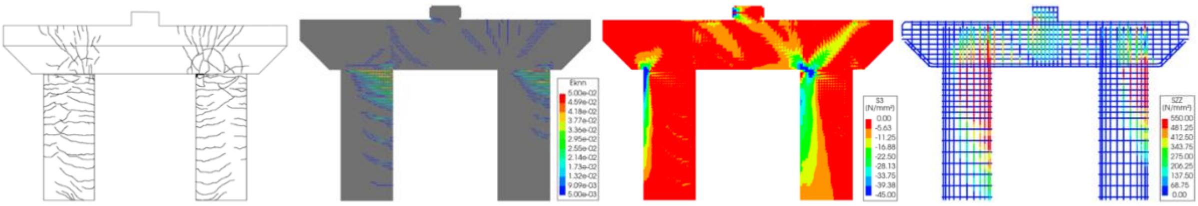

(a) experimental - cracking pattern. (b) numerical - cracking pattern. (c) numerical – principal compressive stress field. (d) numerical – vertical bar stresses.

Figure 14: Damage at 3.46 % drift – 55 mm of displacement.

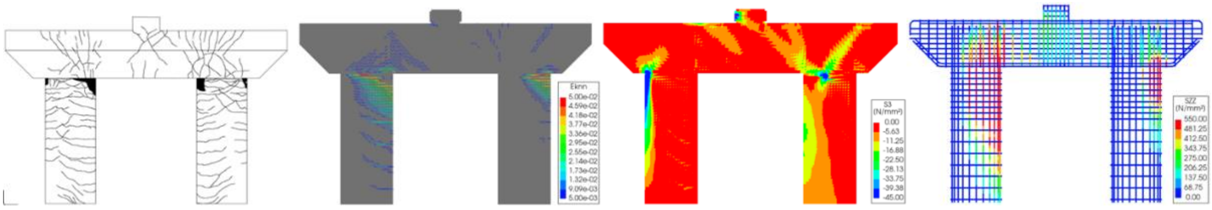

(a) experimental - cracking pattern. (b) numerical - cracking pattern. (c) numerical – principal compressive stress field. (d) numerical – vertical bar stresses.

Figure 15: Damage at 4.84 % drift – 77 mm of displacement.

In Figure 12, for a drift of approximately 0,69 %, the structure begins to lose some lateral stiffness due to the development of some flexural cracks at the top of both columns, along with some localized small cracks in the cap-beam. In Figure 13, for a drift of approximately 2.08%, the structure enters to the yield plateau, where concrete crushing begins in the inner face of the column-to-cap-beam interface, with spalling of the concrete cover. At this stage, the plastic mechanism is fully formed at the top of the columns, with most of the column longitudinal reinforcements yielding, and the confinement reinforcement fulfilling its role. Figure 14 represents the point where the yield plateau ends. From this point ahead, for a drift of approximately 3.46%, the structure no longer supports horizontal loads, continually losing its strength capacity. The structure degradation is severe, with detachment of concrete cover and confinement reinforcements exposed at the column-to-cap-beam interfaces. In Figure 15, for a drift of approximately 4.84%, a significant structure degradation is observed, including the exposure and failure of some longitudinal reinforcements in the plastic hinge zones. This accumulated damage led to the instability of the structure and, therefore, collapse.

6 CONCLUSIONS

- This paper aimed to present a non-linear numerical analysis developed to simulate the behavior of a fully pre-cast substructure system conceived to withstand medium to high seismic forces. Experimental results of the proposed solution in reduced scale were presented and discussed, showing its feasibility for application in high-seismic areas. Numerical results of the same reduced-scale specimen were also presented and compared with the experimental ones, to assess the reliability of the numerical model and its capability to reproduce the phenomena observed experimentally. This will enable the future extrapolation of the experimental results in alternative geometries and reinforcement layouts, while avoiding time loss and high costs that experimental tests require.
- Regarding the experimental test, the specimen presented satisfactory and adequate structural behavior, showing a gradual evolution of damage and ductile behavior. Failure is conditioned by the composite flexural capacity at the top of the columns, as predicted in the design. The propagation of the damage began with the formation of small cracks at the top of the columns, where, with the increase in drift, the formation of plastic hinges was observed. As the horizontal demand increase and the plastic mechanism develop, most of the longitudinal reinforcement of the columns yielded, while the shear and confining reinforcement remained in the elastic range. The failure of the structure occurred with signs of concrete crushing on the inner face of the column, a zone subject to the highest concentration of compressive stresses, following the failure of several longitudinal rebars on the tensioned face.
- The nonlinear numerical analysis effectively simulated the structural behavior observed in the experimental test, showing good agreement. Key phenomena, such as stiffness degradation between cycles, energy dissipation, and the maximum horizontal force were achieved. Some minor divergences were noted, particularly in the initial stiffness and the transition between the elastic and plastic regimes in the positive horizontal demand, likely due to inevitable deformations in the experimental setup during the test.

ACKNOWLEDGMENTS

This work is a result of project iPBRAIL - Innovative Precast Bridges for RAILways, with reference POCI-01-0247-FEDER-039894, co-funded by the European Regional Development Fund (ERDF), through the Operational Programme for Competitiveness and Internationalization (COMPETE 2020) and the Lisbon Regional Operational Programme

(LISBOA 2020), under the PORTUGAL 2020 Partnership Agreement. The authors also acknowledge the financial support: Base - (UIDB/04708/2020) DOI 10.54499/UIDB/04708/2020 (https://doi.org/10.54499/UIDB/04708/2020) and Programmatic - (UIDP/04708/2020) DOI 10.54499/UIDP/04708/2020 (https://doi.org/10.54499/UIDP/04708/2020) of CONSTRUCT financed by national funds through the FCT/MCTES (PIDDAC). This work was also developed within the scope of the project proMetheus – Research Unit on Materials, Energy and Environment for Sustainability, FCT Ref. UID/05975/2020, financed by national funds through the FCT/MCTES.

REFERENCES

[1] V. Popa, A. Papurcu, D. Cotofana, R. Pascu, Experimental testing on emulative connections for precast columns using grouted corrugated steel sleeves. doi: 10.1007/s10518-014-9715-9. Bulletin of Earthquake Engineering, vol. 13, no. 8, 2015.

[2] N. Tullini, F. Minghini, Cyclic test on a precast reinforced concrete column-to-foundation grouted duct connection. doi: 10.1007/s10518-019-00766-2. Bulletin of Earthquake Engineering, vol. 18, no. 4, pp. 1657–1691, Mar. 2020.

[3] M. J. Ameli, C. P. Pantelides, Seismic Analysis of Precast Concrete Bridge Columns Connected with Grouted Splice Sleeve Connectors. doi: 10.1061/(asce)st.1943-541x.0001678. Journal of Structural Engineering, vol. 143, no. 2, 2017.

[4] W. Xu, B. Ma, X. Duan, J. Li, Experimental investigation of seismic behavior of UHPC connection between precast columns and footings in bridges. doi: 10.1016/j.engstruct.2021.112344. Eng. Struct, vol. 239, 2021.

[5] R. Rahman, S. Dirar, Y. Jemaa, M. Theofanous, M. Elshafie. Experimental Behavior and Design of Exterior Reinforced Concrete Beam-Column Joints Strengthened with Embedded Bars. doi: 10.1061/(asce)cc.1943-5614.0000883. Journal of Composites for Construction, vol. 22, no. 6, Dec. 2018.

[6] Z. Wang et al., Quasi-static cyclic tests of precast bridge columns with different connection details for high seismic zones. doi: 10.1016/j.engstruct.2017.12.035. Eng. Struct, vol. 158, 2018.

[7] T. Li, H. Qu, Z. Wang, H. Wei, S. Jiang, Seismic performance of precast concrete bridge columns with quasi-static cyclic shear test for high seismic zones. doi: 10.1016/j.engstruct.2018.03.086. Eng. Struct, vol. 166, 2018.

[8] J. Gao, N. Xiang, J. Li, W. Xu, Cyclic Behavior of Precast Double-Column Bridge Bents with Lap Splice Connections by UHPC. https://doi.org/10.1061/jbenf2.beeng-6041. Journal of Bridge Engineering, vol. 28, no. 7, 2023.

[9] O. Haraldsson, T. Janes, M. Eberhard; J. Stanton, Seismic Resistance of Socket Connection between Footing and Precast Column. https://doi.org/10.1061/(ASCE)BE.1943-5592.0000413. Journal of Bridge Engineering, vol. 18, no. 9, 2013.

[10] L. Carvalho, M. Pimentel, A. Arêde, P. Delgado, N. Vila Pouca, J. Rui Pinto, Design of Pre-cast Two-Column Bents Using Strut-and-Tie Models and Nonlinear Finite Element Analysis. https://doi.org/10.1007/978-3-031-32519-9_174. fib Symposium 2023, LNCE 349, pp. 1732–1741, 2023.

[11] N. Priestley, F. Seible, M. Calvi, Seismic Design and Retrofit of Bridges. 1st ed. John Wiley & Sons Ltd, 1996.

[12] S. Srithran, M. Ingham, Application of strut-and-tie concepts to concrete bridge joints in seismic regions. PCI Journal. 56-90, 2003.

[13] S. Srithran, M. Priestley, F. Seible, Nonlinear finite element analyses of concrete bridge joint systems subjected to seismic action. Finite elements in analysis and design vol. 36, 215-233, 2000.

[14] CSI. SAP2000_v22.1.0 (2020). Finite element program for modelling, analysis, and design of any type of structure. Help documentation of the program, https://www.csiportugal.com/.

[15] (CEN) European commitee for standardization, Eurocode 8 - Design of structures for earthquake resistance - Part 2: Bridges. 2005.

[16] (CEN) European commitee for standardization, Eurocode 8 - Design of structures for earthquake resistance. Part 1: General rules, seismic actions and rules for buildings. 2010.

[17] J. Schlaich, K. Schaefer, and M. Jennewein, Toward a consistent design of structural concrete. PCI Journal, vol. 32, no. 3, 1987.

[18] (CEN) European committee for standardization, Eurocode 1 - Actions on structures. Part 2: Traffic loads on bridges. 2017.

[19] "DIANA," Release 10.4, TNO DIANA BV, Delft, The Netherlands, 2012.

[20] J. Rots, J. Blaauwendraad, Crack models for concrete: Discrete or smeared? Fixed, multi-directional or rotating?. Delft University of Technology, Faculty of Civil Engineering. 1989.

[21] P.H. Feenstra, Computational Aspects of Biaxial Stress in Plain and Reinforced Concrete. PhD thesis, Delft University of Technology, 1993.

[22] R.G. Selby, F.J. Vecchio, Three-dimensional Constitutive Relations for Reinforced Concrete. Tech. Rep. 93-02, Univ. Toronto, dept. Civil Eng., Toronto, Canada, 1993.

[23] D. Hordijk, Local approach to fatigue of concrete. Doctoral Thesis Universiteit Delft, 1991.

[24] M. Menegotto, P. Pinto, Method of analysis for cyclically loaded R.C plane frames including changes in geometry and non-elastic behavior of elements under combined normal force and bending, 1973.

[25] A. Monteiro, A. Arêde, N. Vila Pouca, Seismic behavior of coupled column bridge RC piers: Experimental campaign. DOI: 10.1016/j.engstruct.2016.11.028, 2016.

[26] Fédération internationale du béton., fib Model Code for Concrete Structures 2010. 2013. doi: 10.1002/9783433604090.